Journal of Systems Engineering and Electronics
Vol. 33, No. 2, April 2022, pp.247 – 258

Multiframe track-before-detect method based on velocity filtering in mixed coordinates

WANG Liangliang[1,2] and ZHOU Gongjian[1,2,*]

1. School of Electronics and Information Engineering, Harbin Institute of Technology, Harbin 150001, China;
2. Key Laboratory of Marine Environmental Monitoring and Information Processing, Ministry of Industry and Information Technology, Harbin 150001, China

Abstract: In this paper, a velocity filtering based track-before-detect algorithm in mixed coordinates is presented to address the problem of integration loss caused by inaccurate motion model in polar coordinate sensors. Since the motion of a constant velocity (CV) target is better modeled in Cartesian coordinates, the search of measurements for integration in polar sensor coordinates is carried out according to the CV model in Cartesian coordinates instead of an approximate model in polar sensor coordinates. The position of each cell is converted into Cartesian coordinates and predicted according to an assumed velocity. Then, the predicted Cartesian position is converted back to polar sensor coordinates for multiframe accumulation. The use of the correct model improves integration effectiveness and consequently improves algorithm performance. To handle the weak target with unknown velocity, a velocity filter bank in mixed coordinates is presented. The influence of velocity mismatch on the performance of filter bank is analyzed, and an efficient strategy for filter bank design is proposed. Numerical results are presented to demonstrate the effectiveness of the proposed algorithm.

Keywords: mixed coordinate approach, velocity filtering, multiframe integration, weak target detection, polar sensor coordinate.

DOI: 10.23919/JSEE.2022.000025

1. Introduction

Conventional tracking approaches [1] use thresholded measurements as input. However, the algorithm performance may be degraded when the signal to noise ratio (SNR) is low, since thresholding may discard targets with weak echo intensities. On the contrary, track-before-detect (TBD) methods jointly process consecutive frames of raw sensor data [2−6] or data preprocessed with low detection threshold [7−9] to achieve performance improvement in weak target detection and tracking.

The existing TBD algorithms are categorized into two groups. One is the single frame recursive TBD, such as particle filter based TBD [10−12] and multi-Bernoulli based TBD [13,14]. The other is the multiframe TBD (MF-TBD) or batch processing based method. Dynamic programming based TBD (DP-TBD) [8,15−17] and velocity filter based TBD (VF-TBD) [18−22] are two typical MF-TBD methods.

MF-TBD methods can improve the detection performance of weak targets through energy integration over multiple frames. MF-TBD has been used to detect and track weak moving targets in infrared and optical images [20−24], and is applied to radar systems [15,25−27] and sonar sensors [5,28,29] recently. DP-TBD conducts energy integration by searching for the local maximum value within the feasible region. DP-TBD has an advantage of handling weak maneuvering or motion uncertain targets [30,31]. The integrated envelope of the target is extended to a number of cells, leading to degraded detection performance and estimation accuracy [16,25]. Compared with DP-TBD, VF-TBD integrates target energy by matching the target velocities in raw observation images. The target integrated envelope can be well focused, leading to more effective target detection and parameter estimation.

Most of the existing MF-TBD algorithms [20−23,32] perform measurement collection for multiframe integration based on a linear motion model in measurement plane. When the algorithms are utilized in polar coordinate sensors such as radar and sonar, the model mismatch problem occurs, since the measurements are provided in polar or spherical coordinates, where the common motion with constant Cartesian velocity appears as a nonlinear trajectory in polar sensor coordinates. In [9,33,34], MF-TBD is used to process raw sensor data in

Manuscript received January 08, 2021.
*Corresponding author.
This work was supported by the National Natural Science Foundation of China (61671181).

range-azimuth plane. It is assumed that the target range and azimuth vary linearly with time. However, this assumption is violated especially when the target is near the sensor, leading to poor integration performance. In [25], the constant acceleration model in range coordinate is used for multiframe integration in range-Doppler measurement plane. Although a large searching region can be employed to alleviate the impact of model mismatch in some DP-TBD methods [8,31], a great number of noise measurements involved in the region also lead to degraded performance. To eliminate model mismatch in the range-Doppler domain, the accurate evolution equation of target range-Doppler is derived and energy integration is performed by matching the speed square in [26]. However, this method is limited to TBD for Doppler radars and cannot integrate target echo energy effectively in range-azimuth plane. In many radar or sonar sensor systems, only range and azimuth measurements are provided, it is of significance to investigate effective MF-TBD in range-azimuth plane.

In this paper, a VF-TBD algorithm in mixed coordinates (MC-VF-TBD) is presented for polar coordinate sensors to effectively deal with the raw range-azimuth measurements. In [35], the system transfer function for the mixed coordinate approach is derived, but comprehensive analysis and design of VF-TBD in mixed coordinates are lacking. Compared with [35], in this work, the procedure for multiframe accumulation is provided, the detection strategy is analyzed, and the investigation and design of the velocity filter bank are presented in detail. In the proposed MC-VF-TBD method, the position of each cell is converted into Cartesian coordinates and predicted according to an assumed velocity. The predicted Cartesian position is then converted back to polar sensor coordinates, and the measurement value of the cell is added onto the cell closest to the predicted position for multiframe integration in polar sensor coordinates. This avoids the model inaccuracy caused by motion approximation in sensor coordinates and leads to more effective multiframe integration. The procedure for multiframe integration and the target output envelope are described in detail. To handle the target with unknown velocity, a velocity filter bank in mixed coordinates is presented. The μ-width of target envelope in the velocity domain, representing the envelope width when the intensity equals μ times the peak one, is investigated. Since the use of too few filters may decrease system performance while too many filters may increase the complexity, the μ-width is used to efficiently design the filter bank. This is a tradeoff between system performance and complexity.

The rest of the article is arranged as follows. The measurement model in polar sensor coordinates is presented and the problem of TBD in range-azimuth plane is discussed in Section 2. The integration procedure and detection strategy of the proposed method are provided in Section 3. In Section 4, the velocity filter bank in mixed coordinates is presented in detail. Simulation results are provided in Section 5, followed by conclusions in Section 6.

2. Problem formulation

The observation region is divided into $N_\rho \times N_\theta$ cells with resolution of $\Delta_\rho \times \Delta_\theta$, where N_ρ and N_θ denote the number of cells in range and azimuth, respectively. In the kth frame, the measurement set z_k consists of $N_\rho \times N_\theta$ cells and the echo value of each cell is given by $z_k(n_\rho, n_\theta)$, $n_\rho = 1,2,\cdots,N_\rho$, $n_\theta = 1,2,\cdots,N_\theta$. The kth measurement set z_k is given by

$$z_k = \{z_k(n_\rho, n_\theta) : n_\rho = 1,2,\cdots,N_\rho, n_\theta = 1,2,\cdots,N_\theta\}. \quad (1)$$

The set of all measurements in K frames $Z_{1:K}$ in the processing batch is given by

$$Z_{1:K} = \{z_1, z_2, \cdots, z_K\}. \quad (2)$$

When no target exists, the measurement recorded in cell (n_ρ, n_θ) in frame k is expressed as

$$z_k(n_\rho, n_\theta) = w_k(n_\rho, n_\theta). \quad (3)$$

The proposed multiframe integration procedure can deal with weak targets in arbitrary background. For the convenience of subsequent analysis, the background noise is assumed to be additive independently and identically distributed Gaussian noise. Although the Gaussian case is considered, it will not affect the conclusion of the paper.

When the target exists, the measurement is the sum of the intensities of background noise and target echo, i.e., the $z_k(n_\rho, n_\theta)$ can be expressed as

$$z_k(n_\rho, n_\theta) = s(n_\rho, n_\theta, p_{\rho,k}, p_{\theta,k}) + w_k(n_\rho, n_\theta) \quad (4)$$

where $s(n_\rho, n_\theta, p_{\rho,k}, p_{\theta,k})$ is the target echo envelope in frame k. The Gaussian point spread function is utilized to describe the target energy diffusion, whose parameters depend on sensor characteristics and target size [2,31]. One gets

$$s(n_\rho, n_\theta, p_{\rho,k}, p_{\theta,k}) = A \cdot \exp\left(-\eta_\rho\left(n_\rho - \frac{p_{\rho,k}}{\Delta_\rho}\right)^2 - \eta_\theta\left(n_\theta - \frac{p_{\theta,k}}{\Delta_\theta}\right)^2\right). \quad (5)$$

In the above, A is the peak value of the target echo, $(p_{\rho,k}, p_{\theta,k})$ is the target position in polar sensor coordinates, while η_ρ and η_θ represent the extent of the echo spread in range and azimuth, respectively.

It is of significance to exploit an effective strategy to

detect weak targets with raw range-azimuth measurements. The key to improve the weak target detectability lies in effective integration of target echo values from multiple consecutive frames. The motion model mismatch in sensor coordinates may cause inaccurate integration, especially in the case with high speed targets in low range bins. In [26], the exact target range-Doppler evolution is derived and a speed square matched filter is proposed for TBD in range-Doppler plane. However, this method cannot accurately describe the target motion in range-azimuth plane and is unable to effectively integrate target echo. An accurate motion model in range-azimuth plane will facilitate the interframe integration to a great extent. The multiframe integration strategy is equally important. The method of searching for the local maximum value for multiframe integration [7−9,31] may cause inaccurate integration since the noise value may be larger than target echo intensity under low SNR conditions. In short, motion model mismatch in range-azimuth plane and inaccurate multiframe integration discussed above should be avoided by properly dealing with raw range-azimuth data. In [35], the system transfer function for VF-TBD in mixed coordinates is derived for effective multiframe integration in range-azimuth plane. However, the detailed multiframe integration procedure, detection strategy, filter bank analysis and design are absent in [35]. Thus, this paper is devoted to detailedly investigating VF-TBD in mixed coordinates to obtain effective weak target detection in range-azimuth plane.

3. MC-VF-TBD

To address the above challenges, MC-VF-TBD is presented to obtain effective weak target detection in polar sensor coordinates by matching the constant target Cartesian velocity.

3.1 Integration procedure for MC-VF-TBD

This section provides a detailed description of integration procedure for MC-VF-TBD.

The state of a target moving with constant velocity in Cartesian coordinates is given by

$$\begin{cases} p_{x,k} = p_{x,0} + v_x kT \\ p_{y,k} = p_{y,0} + v_y kT \end{cases} \tag{6}$$

where T denotes the interframe time interval, and $(p_{x,k}, p_{y,k})$ denotes the target position in the kth frame and (v_x, v_y) represents the constant velocity. Equation (6) ignores the process noise, which is always taken into account in traditional tracking algorithms [1]. It is a common assumption in matched filtering methods [20,21], and is feasible within short duration. In the case of large motion uncertainty, the algorithm performance may be reduced on account of the neglect of process noise in (6).

By converting the target state in (6) to sensor coordinates, the polar position of target in frame k is obtained as

$$\begin{cases} p_{\rho,k} = \sqrt{p_{x,k}^2 + p_{y,k}^2} \\ p_{\theta,k} = \arctan\left(\dfrac{p_{y,k}}{p_{x,k}}\right) \end{cases}. \tag{7}$$

A CV target in the x-y plane may not move according to a CV model in polar sensor coordinates due to the nonlinearity between the sensor coordinates and Cartesian coordinates. In MC-VF-TBD, the predicted position of the target in sensor coordinates is obtained accurately according to an assumed velocity using mixed coordinates. This approach avoids the model mismatch, which may result from the motion approximation discussed above. Accordingly, the performance of multiframe integration is improved.

The target energy is assumed to be scattered over quantized cell $(n_{c\rho}, n_{c\theta})$ in frame k. By mapping it into Cartesian coordinates, one gets

$$\begin{cases} n_{cx} = n_{c\rho}\cos(n_{c\theta}\Delta_\theta) \\ n_{cy} = n_{c\rho}\sin(n_{c\theta}\Delta_\theta) \end{cases}. \tag{8}$$

Since no target position information is available in practice, each quantized cell in the observed image will be processed, i.e., $n_{c\rho} = 1, 2, \cdots, N_\rho$, $n_{c\theta} = 1, 2, \cdots, N_\theta$.

The predicted Cartesian position in the last frame K is obtained with assumed velocity (v_x^h, v_y^h) as

$$\begin{cases} n_{px} = n_{cx} + v_x^h (K-k)T \\ n_{py} = n_{cy} + v_y^h (K-k)T \end{cases}. \tag{9}$$

By converting (n_{px}, n_{py}) back to sensor coordinates, the predicted polar position is obtained as

$$\begin{cases} n_{p\rho} = \sqrt{n_{px}^2 + n_{py}^2} \\ n_{p\theta} = \arctan\left(\dfrac{n_{py}}{n_{px}}/\Delta_\theta\right) \end{cases} \tag{10}$$

where $n_{p\rho}$ and $n_{p\theta}$ denote the predicted positions in range and azimuth, respectively. Note that $n_{p\rho}$ and $n_{p\theta}$ may not be integers with $1 \leqslant n_{p\rho} \leqslant N_\rho$ and $1 \leqslant n_{p\theta} \leqslant N_\theta$.

Then, the value in cell $(n_{c\rho}, n_{c\theta})$ in the kth frame is added onto that of the cell closest to the predicted position $(n_{p\rho}, n_{p\theta})$ in the last frame K for multiframe integration. The detailed steps of multiframe accumulation in the proposed method is illustrated in Table 1, where round$(\cdot)$ represents the rounding operator. Since the predicted values of $n_{p\rho}$ and $n_{p\theta}$ may not be integers, the rounding operation enables integration of the energy onto the cell in the last frame. A velocity filter bank can be used to cover the unknown target velocity. The use of filter bank can faci-

litate the multiple targets to be handled in different filters of the bank with different assumed velocities. The multiframe integration in single target scenarios is the same as that in multi-target scenarios. Different from the conventional recursive tracking methods [1], the proposed method can directly perform multiframe integration after setting the filter bank parameters without initialization as in traditional tracking methods.

Algorithm 1 Multiframe integration in MC-VF-TBD

Input $Z_{1:K}=\{z_1,z_2,\cdots,z_K\}$
Initialize integrated value:

$$U(n_\rho,n_\theta)=0,\ n_\rho=1,2,\cdots,N_\rho;n_\theta=1,2,\cdots,N_\theta$$

Set an assumed velocity: $\left(v_x^h,v_y^h\right)$
For $k=1,2,\cdots,K$ **do**
  For $n_{c\rho}=1,2,\cdots,N_\rho$ **do**
    For $n_{c\theta}=1,2,\cdots,N_\theta$ **do**
      Convert to Cartesian coordinates:

$$n_{cx}=n_{c\rho}\cos(n_{c\theta}\Delta_\theta)$$
$$n_{cy}=n_{c\rho}\sin(n_{c\theta}\Delta_\theta)$$

      Predict in Cartesian coordinates:

$$n_{px}=n_{cx}+(K-k)v_x^h$$
$$n_{py}=n_{cy}+(K-k)v_y^h$$

      Convert back to polar coordinates:

$$n_{p\rho}=\sqrt{n_{px}^2+n_{py}^2}$$
$$n_{p\theta}=\arctan\frac{n_{py}}{n_{px}}/\Delta_\theta$$

      Apply rounding operation:

$$n_\rho=\text{round}(n_{p\rho})$$
$$n_\theta=\text{round}(n_{p\theta})$$

      Integrate energy:

$$U(n_\rho,n_\theta)=U(n_\rho,n_\theta)+z_k(n_{c\rho},n_{c\theta})$$

    End
  End
End
Output $U(n_\rho,n_\theta)(n_\rho=1,2,\cdots,N_\rho;n_\theta=1,2,\cdots,N_\theta)$

The procedure for multiframe accumulation in the proposed method is summarized as accurate position prediction in Cartesian coordinates and energy integration in range-azimuth plane. The proposed method is actually a type of three-dimensional matched filter. In contrast to conventional matched filtering based TBD [20,21,24] which is limited to weak target detection in x-y plane, the proposed MC-VF-TBD method can obtain accurate predicted position of the target in range-azimuth plane by matching the constant Cartesian velocity in mixed coordinates. Consequently, the motion model inaccuracy is avoided and the target echo can be integrated adequately in the sensor observed plane. In addition, compared with the matched filtering based TBD in [26] which is proposed for weak target detection in range-Doppler plane, the proposed MC-VF-TBD is capable of effectively dealing with range-azimuth data, and can determine the movement direction of target by respectively matching the Cartesian velocities v_x and v_y in x and y directions, while the method in [26] cannot due to its matching processing of only absolute value of the target speed.

3.2 Detection strategy of MC-VF-TBD

The detection strategy in the proposed method is given by

$$\max_{v_x^h\in\mathfrak{R}_{v_x},v_y^h\in\mathfrak{R}_{v_y}}U(n_\rho,n_\theta)=\max_{v_x^h\in\mathfrak{R}_{v_x},v_y^h\in\mathfrak{R}_{v_y}}\sum_{k=1}^{K}z_k(n_{c\rho,k},n_{c\theta,k})_{v_x^h,v_y^h}\underset{H_0}{\overset{H_1}{\gtrless}}V_T \tag{11}$$

where $(n_{c\rho,k},n_{c\theta,k})_{v_x^h,v_y^h}$ denotes the range-azimuth cell in frame k which can be predicted to cell (n_ρ,n_θ) in the last frame K according to the above mixed coordinate approach with assumed Cartesian velocity $\left(v_x^h,v_y^h\right)$, $\mathfrak{R}_{v_x}$ and $\mathfrak{R}_{v_y}$ are the set of assumed velocities, H_0 and H_1 represent the absence and presence of target, respectively, and V_T is the detection threshold. The threshold can be selected according to the derivation in [22] or estimated through Monte Carlo simulations as described in [6].

The background noise is assumed to be Gaussian distributed with zero mean and covariance σ_w^2, and the mean value of the target echo peak is expressed as A in (5) at the target position. The probability density of $z_k(n_{c\rho,k},n_{c\theta,k})_{v_x^h,v_y^h}$ in (11) (for convenience, z_k is used to represent $z_k(n_{c\rho,k},n_{c\theta,k})_{v_x^h,v_y^h}$ later in this subsection) in the absence or presence of the target is respectively given by

$$\lambda(z_k|H_0)=\frac{1}{\sqrt{2\pi}\sigma_w}\exp\left(-\frac{z_k^2}{2\sigma_w^2}\right) \tag{12}$$

and

$$\lambda(z_k|H_1)=\frac{1}{\sqrt{2\pi}\sigma_w}\exp\left(-\frac{(z_k-A)^2}{2\sigma_w^2}\right) \tag{13}$$

where $\lambda(z_k|H_0)$ and $\lambda(z_k|H_1)$ denote the likelihood function in the absence and presence of the target, respectively.

Then, the logarithm of likelihood ratio is expressed as

$$\Lambda(z_k)=\ln\frac{\lambda(z_k|H_1)}{\lambda(z_k|H_0)}=z_k\frac{A}{\sigma_w^2}-\frac{A^2}{2\sigma_w^2}. \tag{14}$$

By substituting (14) into (11), the detection strategy is rewritten as

$$\max_{v_x^h\in\mathfrak{R}_{v_x},v_y^h\in\mathfrak{R}_{v_y}}\sum_{k=1}^{K}\frac{\sigma_w^2}{A}\left(\Lambda(z_k)+\frac{A^2}{2\sigma_w^2}\right)\underset{H_0}{\overset{H_1}{\gtrless}}V_T. \tag{15}$$

Thus, the detection strategy in (11) is equivalent to

$$\max_{v_x^h\in\Re_{vx},v_y^h\in\Re_{vy}}\sum_{k=1}^{K}\Lambda(z_k)\underset{H_0}{\overset{H_1}{\gtrless}}\frac{2AV_T-A^2K}{2\sigma_w^2} \tag{16}$$

where $\sum_{k=1}^{K}\Lambda(z_k)$ represents the logarithm of likelihood ratio of possible target trajectory. The formula on the left hand side in (16) denotes the maximum logarithm of likelihood ratio, which can be considered as the maximum likelihood estimation of target trajectory. Thus, in the case of Gaussian background noise, the detection strategy (11) in the proposed method is equivalent to the generalized likelihood ratio test [36].

4. Analysis and design of velocity filter bank in mixed coordinates

To deal with a target with an unknown velocity, a velocity filter bank in mixed coordinates is presented in this section, in which each filter assumes a unique velocity to match the actual Cartesian velocity of the target. The theoretical target output envelope in a filter is derived, and the efficient filter bank design is provided.

It is assumed that the peak value A, initial position $(p_{\rho,0},p_{\theta,0})$ and echo spread extents η_ρ and η_θ are constant. In order to facilitate the following derivations, the target echo envelope in frame k in (5) is rewritten as

$$\begin{aligned}&f\left(n_\rho-\frac{p_{\rho,k}-p_{\rho,0}}{\Delta_\rho},n_\theta-\frac{p_{\theta,k}-p_{\theta,0}}{\Delta_\theta}\right)=\\&A\cdot\exp\left(-\eta_\rho\left(n_\rho-\frac{p_{\rho,k}-p_{\rho,0}}{\Delta_\rho}-\frac{p_{\rho,0}}{\Delta_\rho}\right)^2-\right.\\&\left.\eta_\theta\left(n_\theta-\frac{p_{\theta,k}-p_{\theta,0}}{\Delta_\theta}-\frac{p_{\theta,0}}{\Delta_\theta}\right)^2\right).\end{aligned} \tag{17}$$

As derived in [35], the integrated envelope of the target in a filter with assumed velocity $(v_x+\Delta v_x,v_y+\Delta v_y)$ can be obtained through the convolution of target echo (17) and transfer function. One gets

$$\begin{aligned}&u_m(n_\rho,n_\theta,k,\Delta v_x,\Delta v_y)=\\&f\left(n_\rho-\frac{p_{\rho,k}-p_{\rho,0}}{\Delta_\rho},n_\theta-\frac{p_{\theta,k}-p_{\theta,0}}{\Delta_\theta}\right)\cdot\\&\sum_{k_t\in\Re_K}\delta\left(n_\rho+\frac{p^{\Delta}_{\rho,k_t}-p_{\rho,0}}{\Delta_\rho},n_\theta+\frac{p^{\Delta}_{\theta,k_t}-p_{\theta,0}}{\Delta_\theta},k+k_t\right)\end{aligned} \tag{18}$$

where $\Delta v_x=v_x^h-v_x$ and $\Delta v_y=v_y^h-v_y$ are the velocity mismatch errors in range and azimuth, respectively, δ represents the Dirac function, $\Re_K$ represents $\{1-K,\cdots,-1,0\}$, while p^{Δ}_{ρ,k_t} and p^{Δ}_{θ,k_t} are the predicted range and azimuth with assumed velocity $\left(v_x^h,v_y^h\right)$ according to (6) and (7). The term of summation in (18) represents the system transfer function, which is used to obtain the predicted range-azimuth according to an assumed Cartesian velocity for multiframe accumulation in polar coordinates. Similar to the one-dimensional matched filter, the transfer function can be obtained by flipping the target signal in (17).

The target envelope in the velocity domain consists of the maximum output value of each filter in the last frame K as

$$u_v(\Delta v_x,\Delta v_y)=u_m\left(\frac{p_{\rho,K}}{\Delta_\rho},\frac{p_{\theta,K}}{\Delta_\theta},K,\Delta v_x,\Delta v_y\right) \tag{19}$$

where $u_m\left(\frac{p_{\rho,K}}{\Delta_\rho},\frac{p_{\theta,K}}{\Delta_\theta},K,0,0\right)$ is the maximum output value in the filter with matched velocity. The normalized value of (19), i.e., $\bar{u}_v(\Delta v_x,\Delta v_y)=\frac{u_v(\Delta v_x,\Delta v_y)}{u_v(0,0)}$, can be used to represent the integration loss caused by velocity mismatch $(\Delta v_x,\Delta v_y)$, and the loss factor is defined as $\mu=\bar{u}_v(\Delta v_x,\Delta v_y)$. Fig. 1 shows the variation of loss factor in one dimension with Δv representing the velocity mismatch error, where the vertical axis represents the logarithm of the normalized value, i.e., $20\lg\mu$. As illustrated in Fig. 1, the value of loss factor μ decreases as the mismatch error increases.

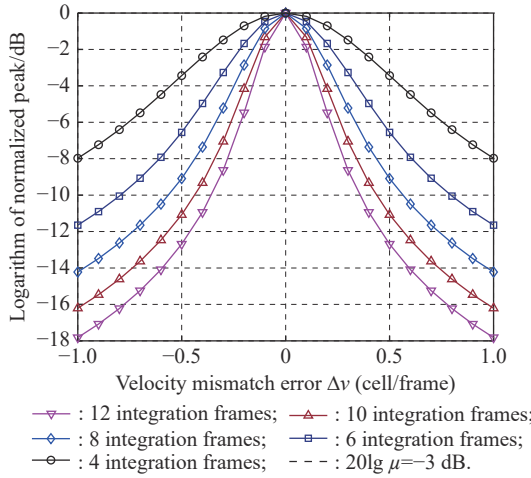

Fig. 1 Curves of μ vs. velocity mismatch error Δv

It is an expected result because the velocity mismatch has an adverse influence on multiframe integration. In addition, the loss factor decreases as the number of accumulated frames K increase, since the prediction error of the target position is amplified by the increased K, leading to degradation in multiframe integration.

The target unknown velocity can be well matched by increasing the number of velocity filters. However, the use of too many filters will increase the system complexity. In this work, the μ-width of envelope in the velocity domain, defined as the envelope width in Fig. 1 when the normalized value equals μ ($\mu\leqslant 1$), is used to efficiently design the filter bank. The theoretical μ-width will be derived later. In [3], the 3 dB width (i.e., the μ-width with

$\mu=1/\sqrt{2}$), which can be considered as the 3 dB velocity resolution property of the filter bank, is used as a compromise between the needs for high system performance and low complexity.

Due to the highly nonlinear motion model in polar sensor coordinates (7), it is hard to derive the exact output of the filter and some approximation is needed. Since the linear model in polar sensor coordinates has the advantage of more tractable analysis, we expand (7) as Taylor series and retain the first order term, the target position in polar sensor coordinates can be approximated as

$$\begin{cases} p_{\rho,k}=\sum\limits_{i=0}^{\infty}\left(\left(\dfrac{p_{\rho,k}^{(i)}}{i!}|_{k=0}\right)k^i\right)\approx p_{\rho,0}+v_{\rho,0}kT \\ p_{\theta,k}=\sum\limits_{i=0}^{\infty}\left(\left(\dfrac{p_{\theta,k}^{(i)}}{i!}|_{k=0}\right)k^i\right)\approx p_{\theta,0}+\dfrac{v_{\theta,0}}{p_{\rho,0}}kT \end{cases} \tag{20}$$

where $\left(p_{\rho,k}^{(i)},p_{\theta,k}^{(i)}\right)$ represents the ith order derivatives of (7), ! denotes the factorial, $v_{\rho,0}$ and $v_{\theta,0}$ respectively denote the initial radial and tangential velocities as

$$v_{\rho,0}=v_x\cos p_{\theta,0}+v_y\sin p_{\theta,0}, \tag{21}$$

$$v_{\theta,0}=v_y\cos p_{\theta,0}-v_x\sin p_{\theta,0}. \tag{22}$$

By substituting (20) into (18), the output envelope in a filter with mismatch error $(\Delta v_x,\Delta v_y)$ can be approximated as

$$u_{ma}(n_\rho,n_\theta,k,\Delta v_x,\Delta v_y)=\sum_{k_t\in\Re_K}f_a\left(n_\rho-\frac{v_{\rho,0}}{\Delta_\rho}kT+\frac{\Delta v_\rho}{\Delta_\rho}k_tT,n_\theta-\frac{v_{\theta,0}}{\Delta_\theta p_{\rho,0}}kT+\frac{\Delta v_\theta}{\Delta_\theta p_{\rho,0}}k_tT\right) \tag{23}$$

where

$$f_a\left(n_\rho-\frac{v_{\rho,0}}{\Delta_\rho}kT,n_\theta-\frac{v_{\theta,0}}{\Delta_\theta p_{\rho,0}}kT\right)=A\cdot\exp\left(-\eta_\rho\left(n_\rho-\frac{p_{\rho,0}+v_{\rho,0}kT}{\Delta_\rho}\right)^2-\eta_\theta\left(n_\theta-\frac{p_{\theta,0}+\frac{v_{\theta,0}}{p_{\rho,0}}kT}{\Delta_\theta}\right)^2\right), \tag{24}$$

$$\Delta v_\rho=\Delta v_x\cos p_{\theta,0}+\Delta v_y\sin p_{\theta,0}, \tag{25}$$

$$\Delta v_\theta=\Delta v_y\cos p_{\theta,0}-\Delta v_x\sin p_{\theta,0}. \tag{26}$$

In the above, f_a is the approximate target echo envelope, Δv_ρ and Δv_θ can be considered as the mismatch errors of the initial velocity in range and azimuth, respectively.

By substituting (23) into (19), the envelope in the velocity domain is approximated as

$$u_{va}(\Delta v_x,\Delta v_y)=\sum_{k_t\in\Re_K}f_a\left(\frac{p_{\rho,K}}{\Delta_\rho}-\frac{v_{\rho,0}KT}{\Delta_\rho}+\frac{\Delta v_\rho k_tT}{\Delta_\rho},\frac{p_{\theta,K}}{\Delta_\theta}-\frac{v_{\theta,0}KT}{\Delta_\theta p_{\rho,0}}+\frac{\Delta v_\theta k_tT}{\Delta_\theta p_{\rho,0}}\right). \tag{27}$$

By expanding (27) as a Taylor series at $\Delta v_\rho=\Delta v_\theta=0$, retaining only the first two terms, and substituting (25) and (26) into (27), the envelope of the target in the velocity domain can be rewritten as

$$u_{va}(\Delta v_x,\Delta v_y)\approx Kf_{pa}+\frac{K(K-1)(2K-1)T^2}{12}\cdot\left(\frac{f_{\rho pa}''}{\Delta_\rho^2}\Delta v_\rho^2+\frac{f_{\theta pa}''}{\Delta_\theta^2p_{\rho,0}^2}\Delta v_\theta^2\right)=q_1\Delta v_x^2+q_2\Delta v_y^2+q_3\Delta v_x\Delta v_y+Kf_{pa} \tag{28}$$

where

$$q_1=N_F\left(\frac{f_{\rho pa}''}{\Delta_\rho^2}\cos^2p_{\theta,0}+\frac{f_{\theta pa}''}{\Delta_\theta^2p_{\rho,0}^2}\sin^2p_{\theta,0}\right), \tag{29}$$

$$q_2=N_F\left(\frac{f_{\rho pa}''}{\Delta_\rho^2}\sin^2p_{\theta,0}+\frac{f_{\theta pa}''}{\Delta_\theta^2p_{\rho,0}^2}\cos^2p_{\theta,0}\right), \tag{30}$$

$$q_3=2N_F\sin p_{\theta,0}\cos p_{\theta,0}\left(\frac{f_{\rho pa}''}{\Delta_\rho^2}-\frac{f_{\theta pa}''}{\Delta_\theta^2p_{\rho,0}^2}\right), \tag{31}$$

$$N_F=\frac{K(K-1)(2K-1)T^2}{12}, \tag{32}$$

where $f_{\rho pa}''$ and $f_{\theta pa}''$ denote the second order partial derivatives of f_a at the target position and f_{pa} denotes its peak value. As illustrated in (28), the envelope of the target in the velocity domain is a quadratic function about the mismatch error of velocity, which is consistent with Fig. 1.

Assume the μ-width [3] is the same in each direction, i.e., $\Delta v_x=\Delta v_y=\Delta v_\mu$. By substituting (28) into (19), the mismatch loss factor μ can be re-expressed as

$$\mu=\frac{(q_1+q_2+q_3)\Delta v_\mu^2+Kf_{pa}}{Kf_{pa}}. \tag{33}$$

For a given mismatch loss μ, the envelope μ-width in the velocity domain is given by

$$\Delta v_\mu=\sqrt{\frac{(\mu-1)Kf_{pa}}{q_1+q_2+q_3}}\sim\left(\frac{1}{K},p_{\rho,0}\right) \tag{34}$$

where $\sim$ represents positive correlation. It can be found from (34) that the value of the μ-width is decreased as the number of integration frames K increases. This is consistent with what is illustrated in Fig. 1. In addition, Δv_μ is positively correlated to the radial distance $p_{\rho,0}$. This is reasonable, since the size of the resolution cell is diverse at different positions of the beam. The farther the cell is from the beginning of the beam, the larger its size is.

We use Δv_μ as the filter bank width to design the velocity filter bank, the number of velocity filters used in the filter bank is

$$N_v = \left\lceil \frac{v_{x\max} - v_{x\min}}{\Delta v_\mu} \right\rceil \cdot \left\lceil \frac{v_{y\max} - v_{y\min}}{\Delta v_\mu} \right\rceil \tag{35}$$

where $(v_{x\min}, v_{x\max})$ and $(v_{y\min}, v_{y\max})$ are the possible velocity ranges in x and y directions, respectively, and $\lceil\cdot\rceil$ denotes the ceiling operator.

Due to the use of a number of filters to deal with unknown target velocity, the computational complexity of the proposed method $O(KN_vN_\rho N_\theta)$ may be a bit high, where O denotes the order of computational complexity, and N_v is the number of filters determined by possible target velocity range and filter bank width in (34). However, the computational complexity of the proposed method is fixed, and not influenced by factors such as the number of targets and clutter models, which is beneficial to system design.

5. Simulation results

In this section, performance of the proposed MC-VF-TBD is evaluated by Monte Carlo simulations. The sampling interval is 10 s, the cell resolution of the sensor is (1 km, 2°), and the possible velocity is assumed to be within (−200 m/s, 200 m/s) in each direction. Two performance measures are used, where detection probability P_d denotes the probability that the position of the target is declared within two cells of the actual one and the threshold is selected according to false alarm probability 10^{-2}. The threshold can be estimated through Monte Carlo simulations [6], or obtained according to the derivation in [22,32]. Table 1 shows the threshold values for different numbers of integration frames in the case of normalized noise covariance $\sigma_w^2 = 1$. Root mean square error (RMSE) is given by

$$\text{RMSE} = \frac{1}{M}\sum_{i=1}^{M}\sqrt{(p_r - p_i)^2} \tag{36}$$

where p_r is the actual target position and p_i is the declared one in the ith simulation while $M = 500$ is the number of simulations.

Table 1 Threshold values for different numbers of integration frames

Number of frames K	Threshold value V_T	Number of frames K	Threshold value V_T
4	5.89	9	11.41
5	7.04	10	12.45
6	8.15	11	13.32
7	9.26	12	13.82
8	10.34	–	–

5.1 Results in single target scenarios

A target is considered in low-range bins with initial Cartesian position (15 km, 10 km) and in high-range bins with initial Cartesian position (350 km, 300 km), respectively. The target Cartesian velocity is (−100 m/s, 100 m/s). The 3 dB filter bank width used is approximately equal to 28 m/s according to (34) or Fig. 1 in Section 4 for six frames.

For comparison, amplitude based DP-TBD (A-DP-TBD) [9] and log-likelihood ratio based DP-TBD (LLR-DP-TBD) [31] are considered.

The targets in low-range and high-range bins have the similar integrated envelope, the integration result in low-range bins is used as an example for comparison. Fig. 2–Fig. 5 show the integration results from two conventional DP-TBD methods, the conventional VF-TBD using the approximate CV model in range-azimuth domain and the proposed MC-VF-TBD with 10 dB SNR and six frames, respectively. As shown in Fig. 2 and Fig. 3, the integrated envelope of the target in DP-TBD methods is extended to many quantized cells caused by its integration strategy based on local maximum value searching. This may degrade the detection and tracking performance of adjacent targets. As shown in Fig. 4, the conventional VF-TBD cannot deal with targets in range-azimuth plane due to the use of the inaccurate model. The target echo cannot be integrated, while the noise value is accumulated after multiframe processing, leading to decreased target SNR. On the contrary, as illustrated in Fig. 5, the proposed MC-VF-TBD can integrate the target echo effectively in mixed coordinates without model mismatch, and the well-focused target envelope facilitates increased detection and estimation performance of algorithm.

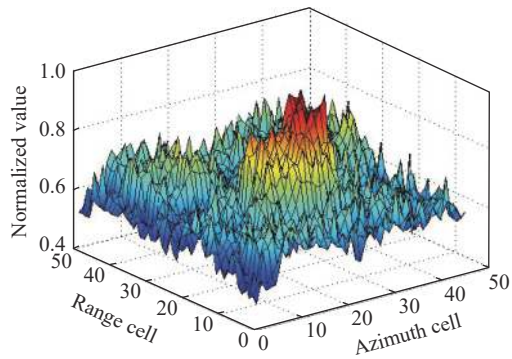

Fig. 2 Integration result from the conventional A-DP-TBD

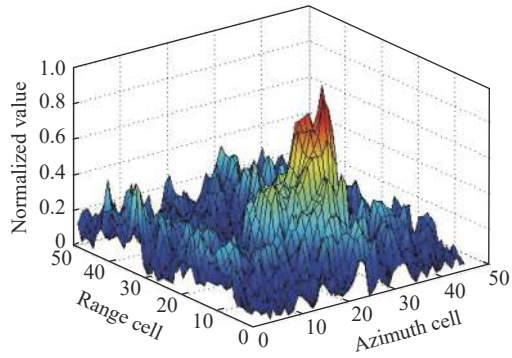

Fig. 3 Integration result from the conventional LLR-DP-TBD

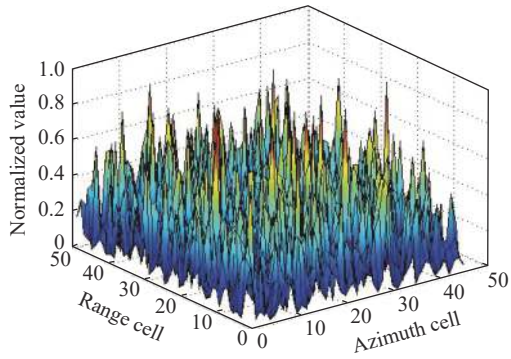

Fig. 4 Integration result from the conventional VF-TBD using approximate CV model in range-azimuth plane

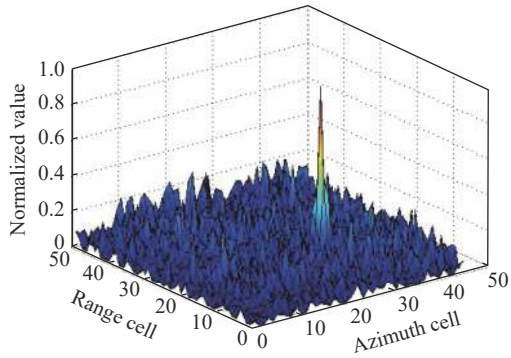

Fig. 5 Integration result from the proposed MC-VF-TBD

Fig. 6 and Fig. 7 show the values of detection probability and RMSE against input SNR in high-range bins, respectively, while Fig. 8 and Fig. 9 show the corresponding results in low-range bins, where σ_v denotes the standard deviation of process noise with unit of m/s^2. As shown in Fig. 6–Fig. 9, the proposed method can yield superior detection and estimation performance over DP-TBD methods. DP-TBD implements multiframe accumulation by searching for the maximum intensity within the possible transition region and adding it to the subsequent frame. This allows the noise value to be increased, adversely affecting target detection. Since the noise value is likely to be larger than target echo intensity at low SNR values, DP-TBD may occur inaccurate integration, causing performance degradation. On the contrary, the proposed MC-VF-TBD integrates the target echo along the target track by matching the target velocity. The echo value of the target can be integrated adequately while the noise value is accumulated slowly because of their independence.

In addition, as illustrated in Fig. 6–Fig. 9, when the target is in low-range bins, the performance of DP-TBD degrades, while that of the proposed MC-VF-TBD does not. In DP-TBD, the motion model approximation in range-azimuth plane may cause model mismatch, which is even more serious in low-range bins and results in significant integration loss. In contrast, the proposed MC-VF-TBD can eliminate model mismatch by performing accurate target position prediction using mixed coordinates. Thus, target echo can be integrated accurately and the algorithm performance is not affected by the distance from the target to the sensor.

It can be found in Fig. 6–Fig. 9 that the performance of the proposed MC-VF-TBD is degraded in the presence of process noise, while DP-TBD does not. It is expected since the strategy of searching for data in a feasible transition region in DP-TBD allows motion uncertainty, while in the proposed method, the velocity matching processing cannot deal well with motion uncertainty but the performance degradation of the proposed MC-VF-TBD is acceptable in case of small process noise.

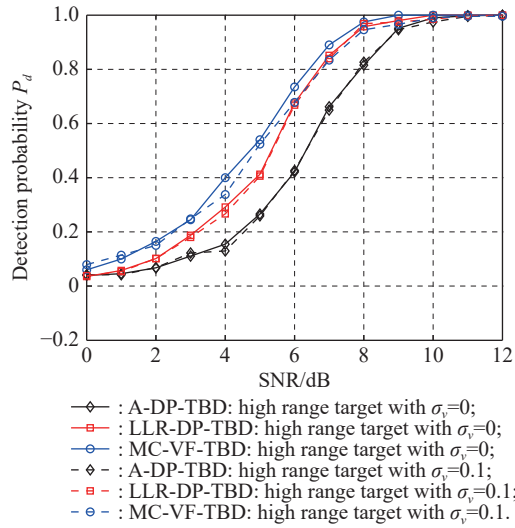

Fig. 6 Detection probabilities vs. input SNR for six integration frames in high range bins

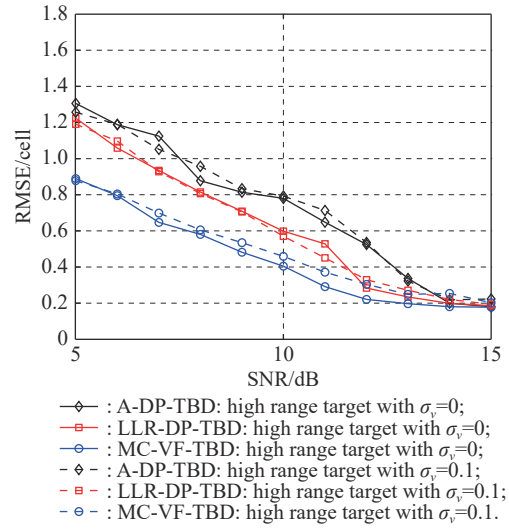

Fig. 7 RMSE values vs. input SNR for six integration frames in high range bins

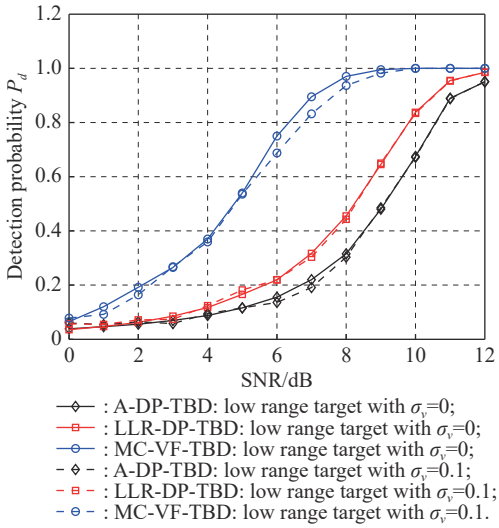

Fig. 8 Detection probabilities vs. input SNR for six integration frames in low range bins

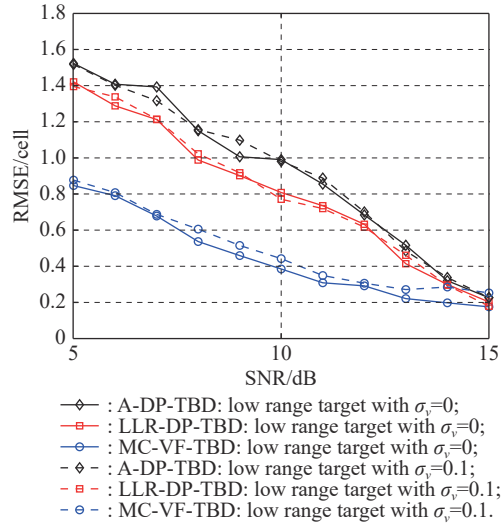

Fig. 9 RMSE values vs. input SNR for six integration frames in low range bins

By comparison, DP-TBD has an advantage of addressing weak targets in the presence of motion uncertainty or maneuver, but suffers from target envelope expansion, while the proposed MC-VF-TBD has higher energy integration efficiency when the actual target model is matched with the assumed one, but the performance may be degraded in the presence of model mismatch.

Fig. 10–Fig. 13 show the performance comparison of three methods against different numbers of integration frames. As illustrated in these figures, detection performance of all three methods is improved since the increase in the number of frames facilitates multiframe energy accumulation. However, the estimation accuracy of DP-TBD cannot be improved by increasing integration frames. It is expected since the integration strategy of DP-TBD (i.e., using the maximum value in the possible transition region for integration) may cause inaccurate integration in each frame when the noise intensity is larger than the target intensity in low SNR conditions, while VF-TBD can eliminate the integration loss by matching the target velocity for data searching.

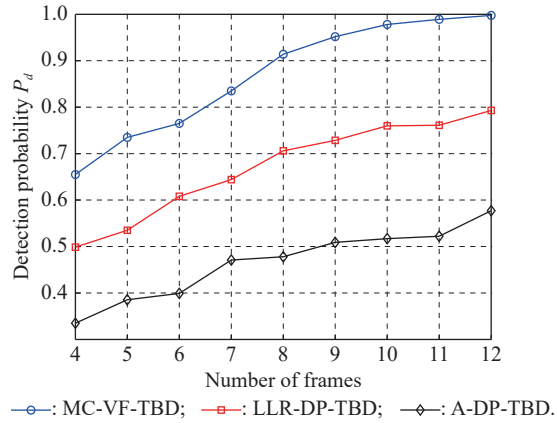

Fig. 10 Detection probabilities vs. number of frames for 6 dB input SNR in high range bins

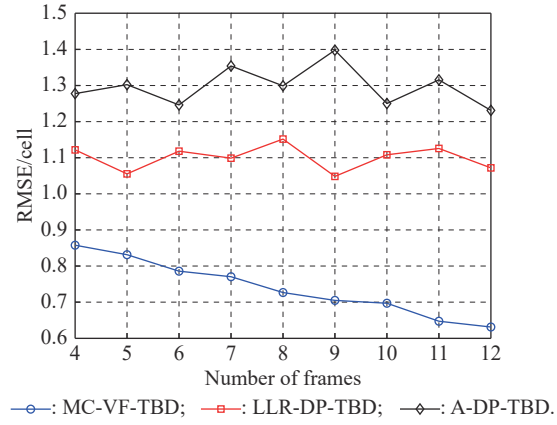

Fig. 11 RMSE values vs. number of integration frames for 6 dB input SNR in high range bins

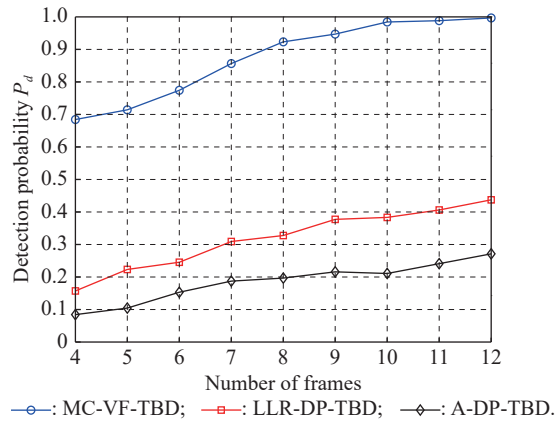

Fig. 12 Detection probabilities vs. number of frames for 6 dB input SNR in low range bins

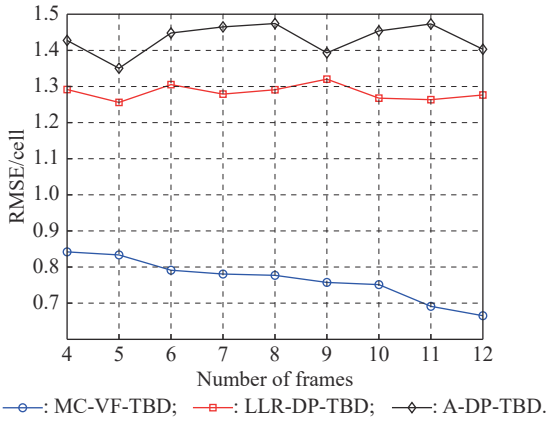

Fig. 13 RMSE values vs. number of integration frames for 6 dB input SNR in low range bins

5.2 Results in multi-target scenarios

The proposed integration method can be used to separately deal with multiple targets in different filters with various assumed velocities. A multi-target scenario with five targets is considered for simulations in this subsection. Their trajectories in polar sensor coordinates are shown in Fig. 14, where targets A and B move with a same Cartesian velocity of (120 m/s, 120 m/s), while targets C, D and E move with a same Cartesian velocity of (0 m/s, −100 m/s). The DP-TBD for multi-target processing (MT-DP-TBD) in [16] is used to compare with the proposed MC-VF-TBD.

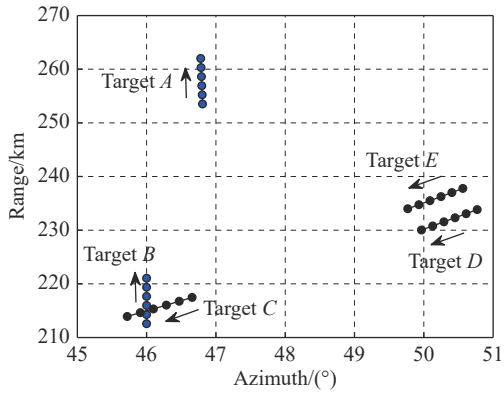

Fig. 14 Trajectories of five targets in a multi-target scenario

Fig. 15 and Fig. 16 show the energy integration of multiple targets for 10 dB input SNR and six frames from MT-DP-TBD and the proposed MC-VF-TBD methods, respectively, where Fig. 16(a) and Fig. 16(b) are the integration results of the proposed filters with matching velocities (120 m/s, 120 m/s) and (0 m/s, −100 m/s), respectively. As shown in Fig. 16(a) and Fig. 16(b), the energy of targets can be integrated accurately in their corresponding filters of MC-VF-TBD and their integrated envelopes are focused. In contrast, the output envelopes of MT-DP-TBD in Fig. 15 are extended to multiple cells, this will cause adjacent targets to interfere with each other, and lead to performance degradation.

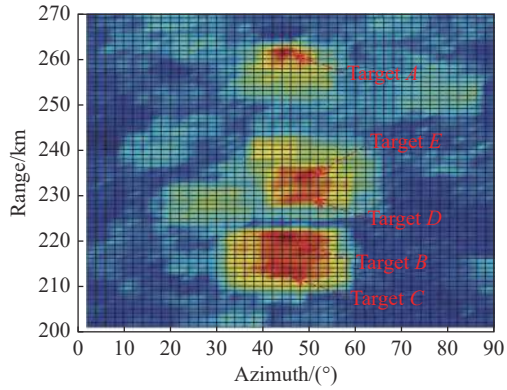

Fig. 15 Multiframe integration in MT-DP-TBD

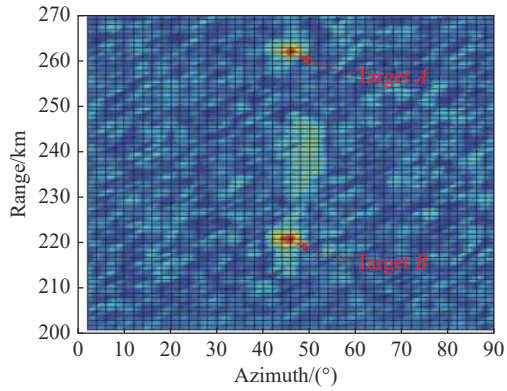

(a) Integration in the filter with matching velocity (120 m/s, 120 m/s)

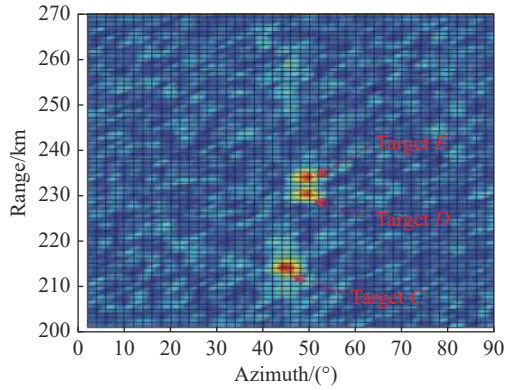

(b) Integration in the filter with matching velocity (0 m/s, −7.00 m/s)

Fig. 16 Multiframe integration in the proposed MC-VF-TBD

Fig. 17 and Fig. 18 show the values of detection probability and RMSE of multiple targets over six frames, respectively. As illustrated in Fig. 17 and Fig. 18, the detection probabilities and RMSE values of the five targets from the proposed MC-VF-TBD are superior to those from MT-DP-TBD. As discussed above, the accurate integration in polar sensor coordinates in the proposed method accounts for the performance superiority.

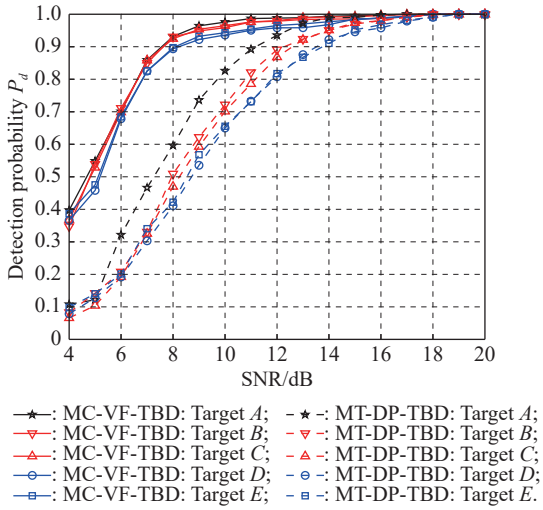

Fig. 17 Detection probabilities of five targets vs. input SNR in case of six integration frames

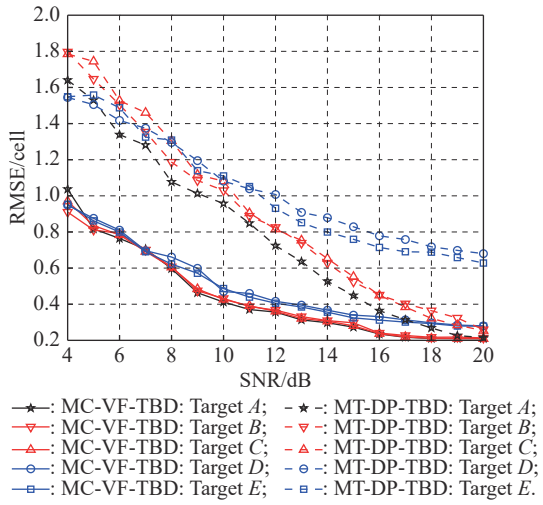

Fig. 18 RMSE values of five targets vs. input SNR in case of six integration frames

As illustrated in Fig. 17 and Fig. 18, the algorithm performance of the MT-DP-TBD method and the proposed MC-VF-TBD method in detecting and tracking the crossing targets (i.e., targets B and C) are both degraded, caused by the mutual interference of targets. In comparison, the effect of target interference can be alleviated in the proposed MC-VF-TBD method by handling targets B and C with various velocities assumed in different filters. Additionally, the target interference also accounts for the algorithm performance degradation in detecting and estimating the targets moving in parallel (i.e., targets D and E). Compared with MT-DP-TBD, this performance degradation is mitigated in the proposed MC-VF-TBD due to its well-focused output envelopes of targets.

It is worth noting that although only several velocities are considered in simulations, the proposed method can handle targets with arbitrary velocities by adjusting the matching velocity range, and the stationary target can be detected in the filter with assumed velocity 0.

6. Conclusions

In this paper, MC-VF-TBD is proposed for polar coordinate sensors to detect and track weak targets, where model mismatch across polar vs. Cartesian coordinates can be avoided due to the use of a mixed coordinate approach. The procedure for multiframe integration is presented in detail. In order to cope with the target with unknown velocity, a velocity filter bank in mixed coordinates is presented. The envelope μ-width in the velocity domain is derived and the effect of velocity mismatch on the filter bank's performance is analyzed. A method used to efficiently design the filter bank is presented to reach a compromise between algorithm accuracy and computational complexity. Simulation results demonstrate the superiority of the proposed algorithm.

References

[1] BAR-SHALOM Y, LI X R, KIRUBARAJAN T. Estimation with applications to tracking and navigation: theory, algorithms, and software. New York: Wiley, 2001.

[2] ORLANDO D, RICCI G, BAR-SHALOM Y. Track-before-detect algorithms for targets with kinematic constraints. IEEE Trans. on Aerospace and Electronic Systems, 2011, 47(3): 1837–1849.

[3] STOCKER A D, JENSEN P D. Algorithms and architectures for imple-menting large-velocity filter banks. SPIE Signal and Data Processing of Small Targets, 1991, 1481: 140–155.

[4] JIANG H C, YI W, CUI G L, et al. Knowledge-based track-before-detect strategies for fluctuating targets in k-distributed clutter. IEEE Sensors Journal, 2016, 16(19): 7124–7132.

[5] DIAMANT R, KIPNIS D, BIGAL E, et al. An active acoustic track-before-detect approach for finding underwater mobile targets. IEEE Journal of Selected Topics in Signal Processing, 2019, 13(1): 104–119.

[6] WANG J H, YI W, HOSEINNEZHAD R, et al. An agile multi-frame detection method for targets with time-varying existence. Signal Processing, 2019, 165: 133–143.

[7] APRILE W A, GROSSI E, LOPS M, et al. Track-before-detect for sea clutter rejection: tests with real data. IEEE Trans. on Aerospace and Electronic Systems, 2016, 52(3): 1035–1045.

[8] GROSSI E, LOPS M, VENTURINO L. A novel dynamic programming algorithm for track-before-detect in radar systems. IEEE Trans. on Signal Processing, 2013, 61(10): 2608–2619.

[9] YI W, KONG L J, YANG J Y. Thresholding process based dynamic programming track-before-detect algorithm. IEICE Trans. on Communications, 2013, E96.B(1): 291–300.

[10] GRCIA-FERNANDEZ A F. Track-before-detect labeled multi-Bernoulli particle filter with label switching. IEEE Trans. on Aerospace and Electronic Systems, 2016, 52(5): 2123–2138.

[11] BOERS Y, MANDAL P K. Optimal particle-filter-based detector. IEEE Signal Processing Letters, 2019, 26(3): 435–439.

[12] GARCIA-FERNANDEZ A F, GRAJAL J, MORELANDE M R. Two-layer particle filter for multiple target detection and tracking. IEEE Trans. on Aerospace and Electronic Systems, 2013, 49(3): 1569–1588.
[13] NGUYEN H V, REZATOFIGHI H, VO B N, et al. Online UAV path planning for joint detection and tracking of multiple radio-tagged objects. IEEE Trans. on Signal Processing, 2019, 67(20): 5365–5379.
[14] VO B N, VO B T, PHAM N T, et al. Joint detection and estimation of multiple objects from image observations. IEEE Trans. on Signal Processing, 2010, 58(10): 5129–5141.
[15] LI W J, YI W, WEN M, et al. Multi-PRF and multi-frame track-before-detect algorithm in multiple PRF radar system. Signal Processing, 2020, 174: 107648.
[16] YI W, MORELANDE M R, KONG L J, et al. An efficient multi-frame track-before-detect algorithm for multi-target tracking. IEEE Journal of Selected Topics in Signal Processing, 2013, 7(3): 421–434.
[17] YI W, JIANG H C, KIRUBARAJAN T, et al. Track-before-detect strategies for radar detection in G0-distributed clutter. IEEE Trans. on Aerospace and Electronic Systems, 2017, 53(5): 2516–2533.
[18] ZHOU G J, WANG L L, KIRUBARAJAN T. A pseudo-spectrum approach for weak target detection and tracking. IEEE Trans. on Aerospace and Electronic Systems, 2019, 55(6): 3394–3412.
[19] WANG L L, ZHOU G J, LI P Y. A complex pseudo-spectrum based velocity filtering method for track-before-detect. Signal Processing, 2020, 174: 107651.
[20] REED I S, GAGLIARDI R M, SHAO H M. Application of three-dimensional filtering to moving target detection. IEEE Trans. on Aerospace and Electronic Systems, 1983, 19(6): 898–905.
[21] KENNEDY H L. Efficient velocity filter implementations for dim target detection. IEEE Trans. on Aerospace and Electronic Systems, 2011, 47(4): 2991–2999.
[22] DRAGOVIC M. Velocity filtering for target detection and track initiation. Edinburgh South Australia: DSTO Systems Sciences Laboratory, 2003:1-55.
[23] ACITO N, CORSINI G, DIANI M. Detection performance loss due to jitter in naval IRST systems. IEEE Trans. on Aerospace and Electronic Systems, 2008, 44(1): 326–338.
[24] LAMPROPOULOS G A, BOULTER J F. Filtering of moving targets using SBIR sequential frames. IEEE Trans. on Aerospace and Electronic Systems, 1995, 31(4): 1255–1267.
[25] DENG X, PI Y, MORELANDE M, et al. Track-before-detect procedures for low pulse repetition frequency surveillance radars. IET Radar, Sonar & Navigation, 2011, 5(1): 65–73.
[26] ZHOU G J, WANG L L. Pseudo-spectrum based speed square filter for track-before-detect in range-Doppler domain. IEEE Trans. on Signal Processing, 2019, 67(21): 5596–5610.
[27] ELHOSHY M, GEBALI F, GULLIVER T A. Expanding window dynamic-programming-based track-before-detect with order statistics in Weibull distributed clutter. IEEE Trans. on Aerospace and Electronic Systems, 2020, 56(4): 2564–2575.
[28] YI W, FU L Z, GARCIA-FERNANDEZ A F, et al. Particle filtering based track-before-detect method for passive array sonar systems. Signal Processing, 2019, 165: 303–314.
[29] EHLERS F, ORLANDO D, RICCI G. Batch tracking algorithm for multistatic sonars. IET Radar, Sonar & Navigation, 2012, 6(8): 746–752.
[30] YI W, FANG Z C, LI W J, et al. Multi-frame track-before-detect algorithm for maneuvering target tracking. IEEE Trans. on Vehicular Technology, 2020, 69(4): 4104–4118.
[31] JIANG H C, YI W, KIRUBARAJAN T, et al. Multiframe radar detection of fluctuating targets using phase information. IEEE Trans. on Aerospace and Electronic Systems, 2017, 53(2): 736–749.
[32] SINGER P F. Performance analysis of a velocity filter bank. SPIE Signal and Data Processing of Small Targets, 1997, 3163: 96–107.
[33] WANG L L, ZHOU G J, HE J, et al. Track-before-detect strategy for radar detection in Rayleigh-distributed noise. Proc. of the 22nd International Conference on Information Fusion, 2019: 1–7.
[34] JIANG H C, YI W, CUI G L, et al. Track-before-detect strategy for HRR radars. Proc. of the IEEE Radar Conference, 2015: 362–367.
[35] WANG L L, ZHOU G J, KIRUBARAJAN T. Track-before-detect technique in mixed coordinates. Proc. of the 21st International Conference on Information Fusion, 2018: 302–307.
[36] KAY S M. Fundamentals of statistical signal processing. Beijing: Publishing House of Electronics Industry, 2006. (in Chinese)

Biographies

WANG Liangliang was born in 1994. He received his B.E. degree in electronic information engineering from Harbin Institute of Technology, Weihai, China in 2016. He is currently pursuing his Ph.D. degree in the School of Electronics and Information Engineering, Harbin Institute of Technology, Harbin, China. From March 2020 to March 2021, he was a visiting Ph.D. student with the Department of Electrical and Computer Engineering, McMaster University, Hamilton, ON, Canada. His research interests include signal processing, target tracking, and parameter estimation, with an emphasis on weak target detection and tracking.
E-mail: awang_liang_liang@163.com

ZHOU Gongjian was born in 1979. He received his B.E., M.E., and Ph.D. degrees in information and communication engineering from Harbin Institute of Technology, Harbin, China, in 2000, 2002, and 2008, respectively. From February 2009 to March 2011, he held a postdoctoral fellowship in the Department of Aerospace Engineering, Harbin Institute of Technology. From April 2011 to May 2012, he was a visiting professor with the Department of Electrical and Computer Engineering, McMaster University, Hamilton, ON, Canada. He is currently a professor with the Department of Electronic Engineering, Harbin Institute of Technology. His research interests include estimation, tracking, detection, information fusion and signal processing.
E-mail: zhougj@hit.edu.cn